CHEMISTRY OF MATERIALS
Article

Chem. Mater. **2010,** *22,* 2155–2163 2155
DOI:10.1021/cm9037796

Polarity and Chirality in Uranyl Borates: Insights into Understanding the Vitrification of Nuclear Waste and the Development of Nonlinear Optical Materials

Shuao Wang,[†] Evgeny V. Alekseev,*[,†,‡] Jie Ling,[†] Guokui Liu,[§] Wulf Depmeier,[‡] and Thomas E. Albrecht-Schmitt*[,†]

[†]*Department of Civil Engineering and Geological Sciences and Department of Chemistry and Biochemistry, 156 Fitzpatrick Hall, University of Notre Dame, Notre Dame, Indiana 46556,* [‡]*Institut für Geowissenschaften, Universität zu Kiel, 24118 Kiel, Germany, and* [§]*Chemical Sciences and Engineering Division, Heavy Elements and Separation Science, Argonne National Laboratory, Argonne, Illinois 60439*

Received December 16, 2009. Revised Manuscript Received January 20, 2010

Four new sodium uranyl borates, α-$Na[(UO_2)_2B_{10}O_{15}(OH)_5]$ (**NaUBO-1**), β-$Na[(UO_2)_2B_{10}O_{15}(OH)_5]$ (**NaUBO-2**), $Na[(UO_2)_2B_{10}O_{15}(OH)_5]\cdot 3H_2O$ (**NaUBO-3**), and $Na[(UO_2)B_6O_{10}(OH)]\cdot 2H_2O$ (**NaUBO-4**), and four new thallium uranyl borates, α-$Tl_2[(UO_2)_2B_{11}O_{18}(OH)_3]$ (**TlUBO-1**), β-$Tl_2[(UO_2)_2B_{11}O_{18}(OH)_3]$ (**TlUBO-2**), $Tl[(UO_2)_2B_{10}O_{16}(OH)_3]$ (**TlUBO-3**), and $Tl_2[(UO_2)_2B_{11}O_{19}(OH)]$ (**TlUBO-4**), have been prepared via the reaction of sodium nitrate or thallium nitrate, uranyl nitrate, and excess boric acid at 190 °C. These compounds share a common structural motif consisting of a linear uranyl, UO_2^{2+}, cation surrounded by BO_3 triangles and BO_4 tetrahedra to create a UO_8 hexagonal bipyramidal environment around uranium. The borate anions bridge between uranyl units to create sheets. Additional BO_3 triangles extend from the polyborate layers and are directed approximately perpendicular to the sheets. In some compounds, these units can link the layers together to yield three-dimensional networks with large pores to house the Na^+ or Tl^+ cations and water molecules. The structures are all noncentrosymmetric and are either polar or chiral. While the uranyl borate layers are noncentrosymmetric in and of themselves, there is also twisting of the interlayer BO_3 groups to reduce the interlayer spacing, producing helical features in some structures. $Na[(UO_2)B_6O_{10}(OH)]\cdot 2H_2O$ and β-$Tl_2[(UO_2)_2B_{11}O_{18}(OH)_3]$, which can be obtained as pure phases, display second-harmonic generation of 532 nm light from 1064 nm light.

Introduction

Borates have attracted the attention of chemists, mineralogists, and materials scientists for decades, and the use of borates for a variety of applications dates back thousands of years.[1] Borate compounds are often remarkably complex owing to the formation of clusters, chains, sheets, and even zeolite-like three-dimensional networks that contain polymerized BO_3 triangles and/or BO_4 tetrahedra in almost limitless combinations.[2,3] While the astonishing crystal chemistry of borates is reason enough to investigate them, there are many practical applications for borates, only two of which will be mentioned here.

Many borates are highly transparent throughout the UV−visible−NIR spectrum. Since neither the BO_3 triangle nor the BO_4 tetrahedron can be placed on centers of inversion (without disorder), some borates adopt noncentrosymmetric structure types.[2−4] When combined with their remarkable transparency and the polarizability of the B−O bonds, they lend themselves well to the development of nonlinear optical materials, especially for deep UV applications. β-BaB_2O_4 is the most widely used of these materials,[5] and its commercial success has spawned the search for new and better noncentrosymmetric borates. These efforts have yielded borate materials with significantly improved properties such as $CsLiB_6O_{10}$.[6]

There is also a second use for borates that is relevant to this present discussion, and that is the vitrification of nuclear waste in borosilicate and borophosphate glasses. The primary waste form for actinides in the United States is borosilicate glasses; in Russia, it is borophosphate glasses.[7] While these waste forms are rather primitive and are undoubtedly not an ideal waste form, they are the ones actually being used as opposed to the more advanced materials such as zircon, garnet, pyrochlore, synroc, and

(1) Woods, W. G. *Environ. Health Perspect.* **1994**, *102*, 5–11.
(2) Burns, P. C.; Grice, J. D.; Hawthorne, F. C. *Can. Mineral.* **1995**, *33*, 1131–1151.
(3) Burns, P. C.; Grice, J. D.; Hawthorne, F. C. *Can. Mineral.* **1999**, *37*, 731–762.
(4) Mori, Y.; Yap, Y. K.; Kamimura, T.; Yoshimura, M.; Sasaki, T. *Opt. Mater.* **2002**, *19*, 1–5.
(5) Chen, C.; Wu, B.; Jiang, A.; You, G. *Sci. Sin.* **1984**, *B7*, 598–604.
(6) Mori, Y.; Sasaki, T. *Bull. Mater. Sci.* **1999**, *22*, 399–403.
(7) Ramsey, W. G. *Glass as a Waste Form and Vitrification Technology: Summary of an International Workshop*; National Academy of Sciences: Washington, DC, 1996.

Published on Web 02/04/2010

monazite that are the subject of current research and debate.[8] It is known that high actinide loadings and slow cooling can lead to the formation of crystals within the glasses.[9] On the basis of dissolution studies on high-borate content glasses, the actinides are apparently primarily interacting with the borate portion of the glass.[9] We have undertaken the task of elucidating the synthesis, structures, and physicochemical properties of actinide borates and recently reported examples of uranyl, neptunyl, and plutonyl borates derived from boric acid flux reactions.[10] One of the eight compounds reported in this work has been briefly communicated.[10] Herein we disclose details on the entire families of sodium and thallium uranyl borates, α-$Na[(UO_2)_2B_{10}O_{15}(OH)_5]$ (**NaUBO-1**), β-$Na[(UO_2)_2B_{10}O_{15}(OH)_5]$ (**NaUBO-2**), $Na[(UO_2)_2B_{10}O_{15}(OH)_5]\cdot 3H_2O$ (**NaUBO-3**), and $Na[(UO_2)B_6O_{10}(OH)]\cdot 2H_2O$ (**NaUBO-4**) and α-$Tl_2[(UO_2)_2B_{11}O_{18}(OH)_3]$ (**TlUBO-1**), β-$Tl_2[(UO_2)_2B_{11}O_{18}(OH)_3]$ (**TlUBO-2**), $Tl[(UO_2)_2B_{10}O_{16}(OH)_3]$ (**TlUBO-3**), and $Tl_2[(UO_2)_2B_{11}O_{19}(OH)]$ (**TlUBO-4**). With one exception,[11] the small family of previously reported uranyl borates[12−17] were prepared at high temperatures in B_2O_3 melts. These high temperatures favor structures with BO_3 triangles, and BO_4 tetrahedra become less common. In contrast, the single uranyl borate prepared at room temperature via slow evaporation, $K_6[UO_2\{B_{16}O_{24}(OH)_8\}]\cdot 12H_2O$, is exceedingly complex, being composed of a cyclic cluster of BO_3 and BO_4 units with a central uranyl core.[11] This present work makes use of the low melting point of boric acid and its use as a reactive flux, to yield complex materials containing polyborates composed of both BO_3 and BO_4 units. Only one of the previously reported uranyl borates, $Ca(UO_2)_2B_2O_6$, is noncentrosymmetric (space group *C*2, polar).[12] The compounds described in this work differ substantially from most uranyl borates in that all of them are noncentrosymmetric. The origin and consequences of the acentricity are detailed within.

Experimental Section

Syntheses. $UO_2(NO_3)_2\cdot 6H_2O$ (98%, International Bio-Analytical Industries), H_3BO_3 (99.99%, Alfa-Aesar), $NaNO_3$ (99.3%, Fisher), and $TlNO_3$ (99.3%, Fisher) were used as received without further purification. Distilled and Millipore filtered water with resistance of 18.2 MΩ·cm was used in all reactions. PTFE-lined autoclaves were used for all reactions. *While the $UO_2(NO_3)_2\cdot 6H_2O$ used in this study contained depleted U, there is really not much difference between depleted uranium and natural abundance uranium, and standard precautions for handling radioactive materials should be followed at all times. There are very old sources of uranyl nitrate that may not be depleted, and enhanced care is warranted for these samples.*

Synthesis of α-$Na[(UO_2)_2B_{10}O_{15}(OH)_5]$ (NaUBO-1), β-$Na[(UO_2)_2B_{10}O_{15}(OH)_5]$ (NaUBO-2), $Na[(UO_2)_2B_{10}O_{15}(OH)_5]\cdot 3H_2O$ (NaUBO-3), and $Na[(UO_2)B_6O_{10}(OH)]\cdot 2H_2O$ (NaUBO-4). $UO_2(NO_3)_2\cdot 6H_2O$, boric acid, and sodium nitrate with 10 different Na:U:B molar ratios (1:1:6, 1:1:10, 1:1:15, 2:1:8, 2:1:15, 3:1:8, 3:1:15, 4:1:15, 5:1:15, and 6:1:15; 1 mmol of $UO_2(NO_3)_2\cdot 6H_2O$ was used in each reaction) were loaded into ten 23 mL autoclaves. The autoclaves were sealed and heated to 190 °C in a box furnace for 24 h. The autoclaves were then cooled down to room temperature at a rate of 5 °C/h. All the products were washed with boiling water to remove excess boric acid, followed by rinsing with methanol. Crystals in the form of tablets and prisms with light yellow-green coloration were collected for the first four reactions, and only prisms were found in the last six reactions. Single crystal X-ray diffraction and powder X-ray diffraction studies reveal that **NaUBO-1** and **NaUBO-2** form as the major products of the first 4 ratios. Whereas **NaUBO-3** only occurs in 1:1:15 ratio reaction, and **NaUBO-4** exists in all 10 reactions and can be found as a pure phase for the last 6 reaction ratios.

Synthesis of α-$Tl_2[(UO_2)_2B_{11}O_{18}(OH)_3]$ (TlUBO-1), β-$Tl_2[(UO_2)_2B_{11}O_{18}(OH)_3]$ (TlUBO-2), $Tl[(UO_2)_2B_{10}O_{16}(OH)_3]$ (TlUBO-3), and $Tl_2[(UO_2)_2B_{11}O_{19}(OH)]$ (TlUBO-4). $UO_2(NO_3)_2\cdot 6H_2O$, boric acid, and thallium nitrate with eight different Tl:U:B molar ratios (1:1:8, 1:1:15, 1:1:22, 2:1:8, 2:1:15, 2:1:22, 3:1:15, 3:1:22; 1 mmol of $UO_2(NO_3)_2\cdot 6H_2O$ was used in each reaction) were loaded into eight 23 mL autoclaves. The autoclaves were sealed and heated to 190 °C in a box furnace for 3 days. The autoclaves were then cooled down to room temperature at a rate of 5 °C/h. All the products were washed with boiling water to remove excess boric acid, followed by rinsing with methanol. Crystals in the form of tablets, prisms, and blocks with light yellow coloration were collected for all eight reactions. Single crystal X-ray diffraction and powder X-ray diffraction studies reveal that **TlUBO-2** occurs in all eight ratio reactions and is the only phase in the 1:1:22 and 2:1:22 reactions. **TlUBO-3** can only be found in the 1:1:8 reactions; however, **TlUBO-4** and **TlUBO-1** exist in all reactions except the 1:1:22 and 2:1:22 reactions.

Crystallographic Studies. Single crystals of all eight **NaUBO** and **TlUBO** phases were mounted on glass fibers and optically aligned on a Bruker APEXII CCD X-ray diffractometer or a Bruker APEXII Quazar X-ray diffractometer using a digital camera. Initial intensity measurements were either performed using a IμS X-ray source, a 30 W microfocused sealed tube (MoKα, λ = 0.71073 Å) with high-brilliance and high-performance focusing Quazar multilayer optics, or a standard sealed tube with a monocapillary collimator. Standard APEXII software was used for determination of the unit cells and data collection control. The intensities of reflections of a sphere were collected by a combination of four sets of exposures (frames). Each set had a different φ angle for the crystal and each exposure covered a range of 0.5° in ω. A total of 1464 frames were collected with an exposure time per frame of 10 to 50 s, depending on the crystal. The SAINT software was used for data integration including Lorentz and polarization corrections. Semiempirical absorption corrections were applied using the program SADABS.[18] Selected crystallographic information are listed in Tables 1 and 2. Atomic coordinates, bond

(8) (a) Krivovichev, S. *Minerals as Advanced Materials I*; Springer: Heidelberg, 2008. (b) Farnan, I.; Cho, H.; Weber, W. J. *Nature* **2007**, *445*, 190–193. (c) Ewing, R. C. *Nature* **2007**, *445*, 161–162. (d) Ewing, R. C. *Proc. Natl Acad. Sci. U.S.A.* **1999**, *96*, 3432–3439.
(9) Meaker, T. F. *Neptunium Immobilization and Recovery Using Phase Separated Glasses*; U.S. Department of Energy, 1996.
(10) Wang, S.; Alekseev, E. V.; Ling, J.; Skanthakumar, S.; Soderholm, L.; Depmeier, W.; Albrecht-Schmitt, T. E. *Angew. Chem., Int. Ed.* **2010**, *49*, 1263.
(11) Behm, H. *Acta Crystallogr., Sect. C* **1985**, *41*, 642–645.
(12) Gasperin, M. *Acta Crystallogr., Sect. C* **1987**, *43*, 1247–1250.
(13) Gasperin, M. *Acta Crystallogr., Sect. C* **1987**, *43*, 2031–2033.
(14) Gasperin, M. *Acta Crystallogr., Sect. C* **1987**, *43*, 2264–2266.
(15) Gasperin, M. *Acta Crystallogr., Sect. C* **1988**, *44*, 415–416.
(16) Gasperin, M. *Acta Crystallogr., Sect. C* **1989**, *45*, 981–983.
(17) Gasperin, M. *Acta Crystallogr., Sect. C* **1990**, *46*, 372–374.
(18) Sheldrick, G. M. *SADABS 2001*, Program for absorption correction using SMART CCD based on the method of Blessing: Blessing, R. H. *Acta Crystallogr.* **1995**, *A51*, 33–38.

Table 1. Crystallographic Data for α-$Na[(UO_2)_2B_{10}O_{15}(OH)_5)]$ (NaUBO1), β-$Na[(UO_2)_2B_{10}O_{15}(OH)_5]$ (NaUBO2), $Na[(UO_2)_2B_{10}O_{15}(OH)_5]\cdot 3H_2O$ (NaUBO3), and $Na[(UO_2)B_6O_{10}(OH)]\cdot 2H_2O$ (NaUBO4)

Compound	NaUBO1	NaUBO2	NaUBO3	NaUBO4
Mass	991.15	991.15	1039.15	566.89
Color and habit	Yellow-Green, tablet	Yellow-Green, tablet	Yellow-Green, tablet	Yellow-Green, prism
Space group	$P3_2$ (No. 145)	*Cc* (No. 9)	$P3_121$ (No. 152)	*Cc* (No. 9)
a (Å)	6.4334(14)	11.1473(11)	6.4410(4)	6.3905(9)
b (Å)	6.4334(14)	6.4441(6)	6.4410(4)	11.139(2)
c (Å)	35.586(0)	23.756(2)	41.836(2)	15.987(2)
α (°)	90	90	90	90
β (°)	90	90.870(1)	90	92.777(2)
γ (°)	120	90	120	90
V (Å^3)	1275.5(4)	1706.3(3)	1503.1(2)	1136.7(3)
Z	3	4	3	2
T (K)	293(2)	293(2)	293(2)	293(2)
λ (Å)	0.71073	0.71073	0.71073	0.71073
Maximum 2θ (°)	28.72	28.73	28.92	34.93
ρ calcd (g/cm^{-3})	3.871	3.858	3.444	3.394
μ (Mo *K*α, cm^{-1})	191.83	191.20	162.98	144.67
R(*F*)for $F_o^2 > 2\sigma(F_o^2)^a$	0.0364	0.0335	0.0408	0.0270
*R*w(F_o^2)^b	0.0669	0.0663	0.1023	0.1073

$^aR(F) = \Sigma||F_0|-|F_c||/\Sigma|F_0|$ $^bR(F_0^2) = [\Sigma w(F_0^2-F_c^2)^2/\Sigma w(F_0^4)]^{1/2}$

Table 2. Crystallographic Data for α-$Tl_2[(UO_2)_2B_{11}O_{18}(OH)_3]$ (TlUBO-1), β-$Tl_2[(UO_2)_2B_{11}O_{18}(OH)_3]$ (TlUBO-2), $Tl[(UO_2)_2B_{10}O_{16}(OH)_3]$ (TlUBO-3), and $Tl_2[(UO_2)_2B_{11}O_{19}(OH)]$ (TlUBO-4)

Compound	TlUBO-1	TlUBO-2	TlUBO-3	TlUBO-4
Mass	1403.71	1403.71	1156.53	1387.71
Color and habit	Yellow, block	Yellow, plate	Yellow, plate	Yellow, prism
Space group	*P*1	*Cc*	*Cc*	*Cc*
a (Å)	6.4488(3)	6.4506(8)	11.1568(15)	11.1689(10)
b (Å)	7.1595(3)	11.2100(14)	6.4424(9)	6.4541(6)
c (Å)	11.0929(5)	27.531(4)	25.328(4)	28.216(2)
α (°)	94.83	90	90	90
β (°)	90.01	94.387(1)	95.919(1)	99.146(1)
γ (°)	97.13	90	90	90
V (Å^3)	506.37(4)	1985.0(4)	1810.8(4)	2008.1(3)
Z	1	4	4	4
T (K)	100(2)	296(2)	293(2)	293(2)
λ (Å)	0.71073	0.71073	0.71073	0.71073
Maximum 2θ (°)	28.70	28.75	28.77	28.81
ρ calcd (g cm^{-3})	4.603	4.697	4.242	4.590
μ (Mo *K*α)	319.30	325.82	268.42	322.00
R(*F*)for $F_o^2 > 2\sigma(F_o^2)^a$	0.0260	0.0302	0.0325	0.0269
*R*w(F_o^2)^b	0.0646	0.0561	0.0755	0.0621

$^aR(F) = \Sigma||F_0|-|F_c||/\Sigma|F_0|$ $^bR(F_0^2) = [\Sigma w(F_0^2-F_c^2)^2/\Sigma w(F_0^4)]^{1/2}$

distances, and additional structural information are provided in the Supporting Information (CIF files).

Powder X-ray Diffraction. Powder X-ray diffraction patterns of the products of all reactions were collected on a Scintag theta−theta diffractometer equipped with a diffracted-beamed monochromatic set for Cu Kα (λ = 1.5418 Å) radiation at room temperature in the angular range from 10° to 80° (2θ) with a scanning step width of 0.05° and a fixed counting time of 1 s/step. The collected patterns were compared with those calculated from single crystal data using ATOMS (see Supporting Information).

Thermogravimetric Analysis (TGA). TGA measurements for the pure phase **NaUBO-4** were conducted using a NetzschTG209F1 Iris thermal analyzer. A sample of **NaUBO-4** was loaded into an alumina crucible and heated from 20 to 900 °C at a rate of 5 °C/min under flowing nitrogen gas. The thermogram can be found in the Supporting Information.

Second-Harmonic Generation Measurements. Powder second-harmonic generation (SHG) measurements were performed on a Kurtz-Perry nonlinear optical system.[19] A Q-switched Nd:YAG laser (Continuum Surelite I-10), operated at 10 Hz, provided the 1064 nm light used for all measurements. The SHG intensity was recorded from a polycrystalline sample of **NaUBO-4** and **TlUBO-2**. No index of refraction matching fluid was used in these experiments. The SHG light at 532 nm was collected in reflection, selected by a narrow band-pass interference filter (Pomfret), and detected by a photomultiplier tube (RCA 1P28). A near normal incidence beam splitter reflected a small fraction of the laser beam onto a pyroelectric detector (Molectron J3-05) that was used as a laser pulse energy monitor. A digital storage oscilloscope (Tektronix TDS 640A) signal averaged and recorded both the SHG and the incident laser energy signals. Average laser power was measured separately with a calibrated Scientech volume absorber calorimeter. *As an important note for other investigators interested in the nonlinear optical properties of radioactive materials: The practice of grinding and sieving powders so that comparisons can be made with reference materials of similar particle size is unsafe. We ground and sieved a less-radioactive thorium compound inside a glovebox and then surveyed the interior of the glovebox. There was a uniform contamination of 50 dpm on every surface tested. We recommend discontinuation of this practice immediately. It is enough*

(19) Kurtz, S. K.; Perry, T. T. *J. Appl. Phys.* **1968**, *39*, 3798–3813.

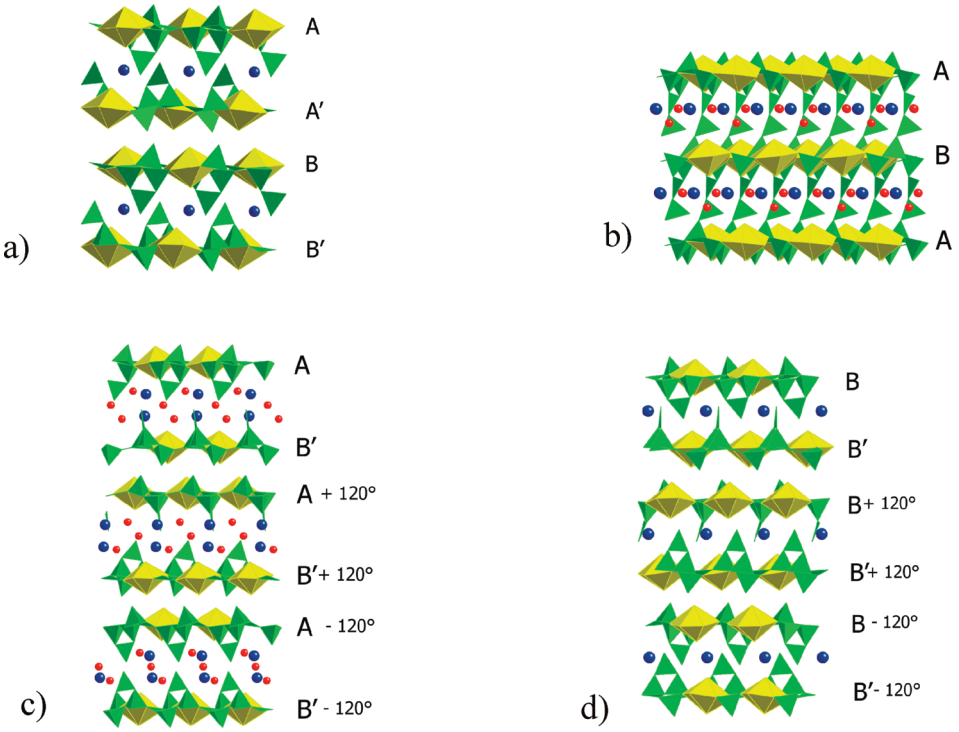

Figure 1. Views of the crystal structures of α-Na[$(UO_2)_2B_{10}O_{15}(OH)_5$)] (**NaUBO-1**) (a), *β*-Na[$(UO_2)_2B_{10}O_{15}(OH)_5$] (**NaUBO-2**) (d), Na[$(UO_2)_2B_{10}O_{15}$-$(OH)_5$]·$3H_2O$ (**NaUBO-3**) (c), and Na[$(UO_2)B_6O_{10}(OH)$]·$2H_2O$ (**NaUBO-4**) (b). UO_8 hexagonal bipyramids are shown in yellow, BO_3 and BO_4 units in green, Na^+ cations in blue, and water molecules in red.

to say that there is or is not SHG activity. The magnitude is not important enough to risk the health of researchers.

Results and Discussion

Synthesis. Molten boric acid is an exceedingly good reactive-flux for the preparation of borate compounds at relatively low temperatures.[20] We have tried for more than a decade to prepare actinide borates compounds and have been largely unsuccessful because we employed hydrothermal conditions as the preparative method. Actinide borates are difficult to prepare by traditional methods in general because water competes very successfully with borate for inner-sphere coordination sites with these metals under most conditions. In fact, many borates that occur naturally are found in evaporate deposits in arid regions.[2,3] This synthetic challenge can be overcome by either removing water entirely from the system in high-temperature solid-state reactions[12−17] or slow evaporations[11] or by reducing the dielectric constant of water by heating to create hydrothermal conditions. Mild hydrothermal conditions are not sufficient for preparing new uranyl borates. Supercritical water works better, but one has to question the wisdom of heating radioactive materials to high temperatures and high pressures. Boric acid has proven to be an ideal solution to this problem, and we have more than 30 actinide borates in hand.

The formation of four phases in the **NaUBO** system is found to be a stoichiometrically driven reaction, which means that the formation of the four compounds is related to the molar ratio of sodium, uranium, and borate in the starting materials. The **NaUBO-1**, **NaUBO-2**, and **NaUBO-3** phases have a Na:U ratio of 1:2 and are favored in the reactions that have a lower Na:U ratio. When increased amounts of sodium are present in the reaction mixture, **NaUBO-4** becomes more favored and can be made as a pure phase. The reaction yields increase with reaction time. One day reactions are appropriate for screening product composition, but only lead to low isolated yields. The yield maximizes after seven d ays at 72% for **NaUBO-4**. TGA analysis suggests that **NaUBO-4** loses water near the synthesis temperature but that there are no further changes until 500 °C.

As found in the sodium system, the formation of four phases in the **TlUBO** system is found to be a stoichiometrically driven reaction, which means that the formation of the four compounds is related to the molar ratio of thallium, uranium, and borate in the starting materials. The **TlUBO-3** phase has a Tl:U ratio of 1:2 and can only be made in the reaction that has a low Tl:U ratio (1:1) for the starting materials. When increased amounts of thallium are present in the reaction mixture, **TlUBO-1**, **TlUBO-2**, and **TlUBO-4**, which have a high Tl:U ratio (1:1), become more favored, and **TlUBO-3** can be made as a pure phase in the high borate concentration reactions (U:B = 1:22). The 1:1:22 (Tl:U:B) reaction has a moderate yield for **TlUBO-3**, of about 42% based on the uranium.

General Comments of Topology and Polymorphism in Sodium Uranyl Borates. Fragments of the crystal structures of **NaUBO-1**, **NaUBO-2**, **NaUBO-3**, and **NaUBO-4** are depicted in Figure 1a−d. Within these structures we

(20) (a) Yang, T.; Sun, J.; Eriksson, L.; Li, G.; Zou, X.; Liao, F.; Lin, J. *Inorg. Chem.* **2008**, *47*, 3228–3233. (b) Li, L.; Wang, Y.; Jin, X.; Li, G.; Wang, Y.; You, L.; Lin, J. *Chem. Mater.* **2002**, *14*, 4963–4968.

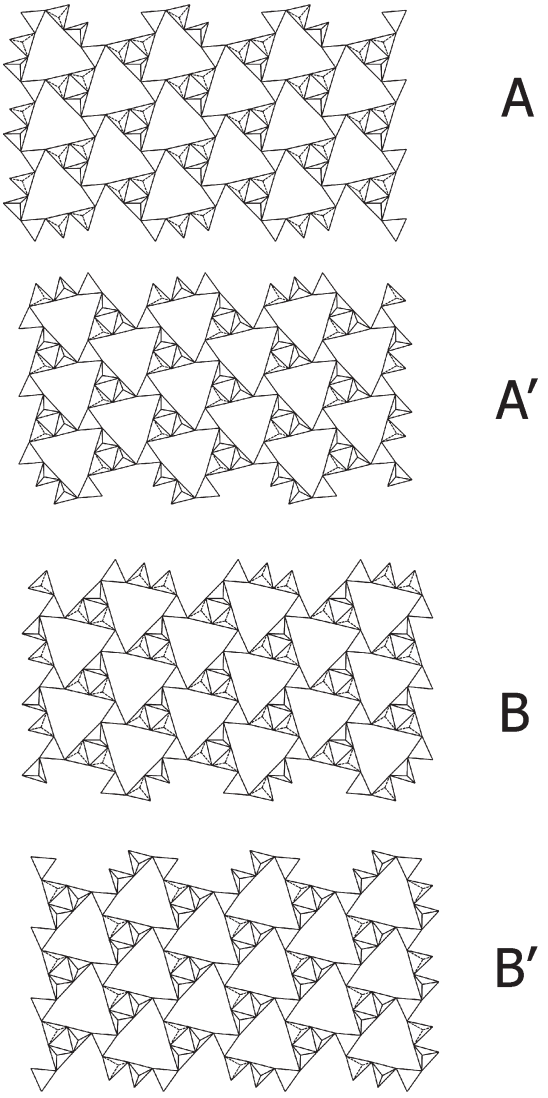

Figure 2. Skeletal representation of the polyborate sheet found in the structure of α-Na[$(UO_2)_2B_{10}O_{15}(OH)_5$)] (**NaUBO-1**).

can separate sheets directed perpendicular to *c*. All these sheets are based on boron oxo-groups (green tetrahedra and triangles) and 6-fold coordinated uranyl groups (yellow hexagonal bipyramids). We will consider only the boron-based part of these sheets because the uranyl groups are similar in all of them. There are four (in general) different types of sheets—A, A′, B, and B′ (the structure of these layers is taken from **NaUBO-1** and presented in Figure 2 in skeletal mode). All of them are strongly related (based on the same structural fragments) and can be transformed into each other using simple crystallographic operations. In these structures we can separate fragments that will be unique units and at the same time represented in all the structural features. These fragments are shown in Figure 3a. In the center of these units are flat BO_3 triangles (using the topological symbols, these are shown as black triangles). These groups are connected by a vertex with groups consisting of three BO_4 tetrahedra. These groups are located differently in A and B, and this is shown in the topological description by solid lines. In each of these groups one BO_4 tetrahedra is

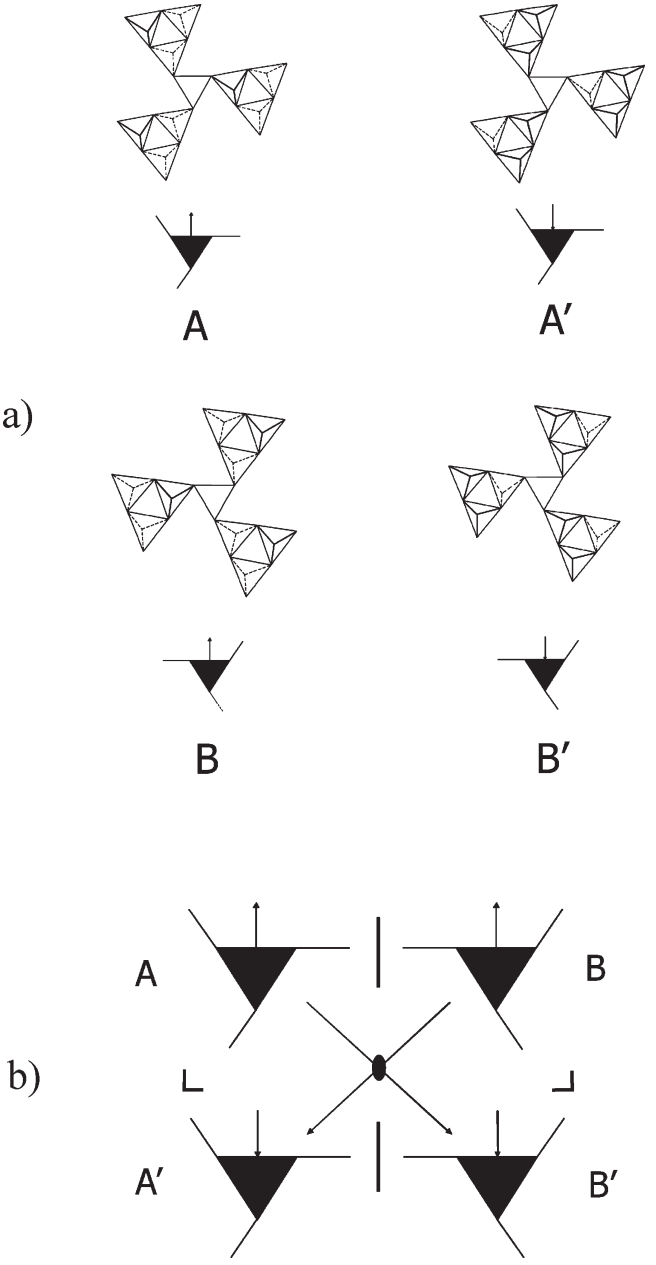

Figure 3. Characteristic fragments of the oxoborate sheets (a) and views of the crystallographic transformations that relate the different sheets (b) in α-Na[$(UO_2)_2B_{10}O_{15}(OH)_5$)] (**NaUBO-1**), β-Na[$(UO_2)_2B_{10}O_{15}$-$(OH)_5$] (**NaUBO-2**), Na[$(UO_2)_2B_{10}O_{15}(OH)_5$]·$3H_2O$ (**NaUBO-3**), and Na[$(UO_2)B_6O_{10}(OH)$]·$2H_2O$ (**NaUBO-4**). From part a we can see that groups A and A′ are mostly similar and defer only in the direction of BO_4 tetrahedra. These two modifications are related by the mirror plane parallel to the sheets (see part b). A and B layer types are enantiomorphic and can be transformed by the plane mirror plane that is perpendicular to the sheets (part b). The relationship between B and B′ is similar to the relationship between A and A′. Finally, A (or B) can be transformed to B′ (or to A′) by the simple 2-fold axis that is parallel to the plane of the sheets.

directed "up" (arrow up on topology diagram) or "down" (arrow down on topology diagram); the other two are directed into the opposite side. From Figure 3a we can see that groups A and A′ are mostly similar and defer only in direction of BO_4 tetrahedra. These two modifications are related by the mirror plane parallel to the sheets (see Figure 3b). A and B layer types are enantiomorphic and can be transformed by the plane mirror plane that is

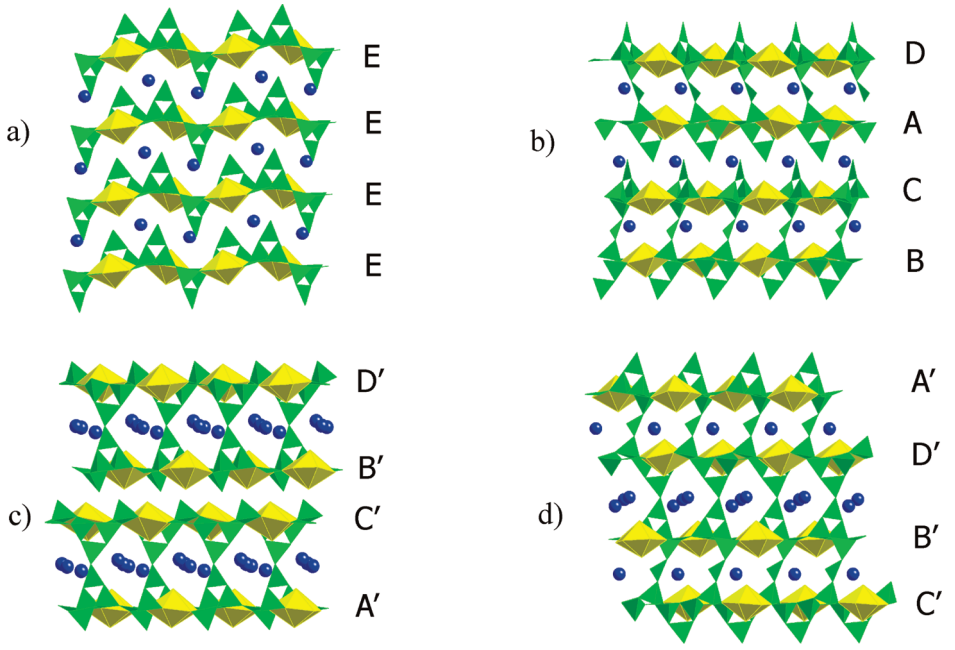

Figure 4. Views of the crystal structures of α-$Tl_2[(UO_2)_2B_{11}O_{18}(OH)_3]$ (**TlUBO-1**) (a), β-$Tl_2[(UO_2)_2B_{11}O_{18}(OH)_3]$ (**TlUBO-2**) (b), $Tl[(UO_2)_2B_{10}O_{16}(OH)_3]$ (**TlUBO-3**) (c), and $Tl_2[(UO_2)_2B_{11}O_{19}(OH)]$ (**TlUBO-4**) (d). UO_8 hexagonal bipyramids are shown in yellow, BO_3 and BO_4 units in green, and Tl^+ cations in blue.

perpendicular to the sheets (Figure 3b). The relationship between B and B′ is similar to the relationship between A and A′. Finally, A (or B) can be transformed to B′ (or to A′) by the simple 2-fold axis that is parallel to the plane of the sheets. All these transformations are schematically presented in Figure 3b.

If we look again at Figure 1, we can find that phases **NaUBO-1** and **NaUBO-4** are crystallized in polar space groups that are based on both enantiomorphic sheets—A and B. Compounds **NaUBO-2** and **NaUBO-3** are crystallized in polar and chiral space groups and consist only of A or B layers (and B′), and each third layer is formed by a previous rotation of 120° (see Figures 1 c,d). The structural difference in polymorphic modifications (**NaUBO-1** and **NaUBO-2**) has the same nature. The α-$Na[(UO_2)_2B_{10}O_{15}(OH)_5)]$ (**NaUBO-1**) phase is based on A,A′-B,B′-A,A′-... packing, and the β-$Na[(UO_2)_2B_{10}O_{15}(OH)_5]$ (**NaUBO-2**) phase on B,B′-B,B′-B,B′-... packing.

Finally, in all four compounds there are BO_3 triangles that are directed between the layers. In all of the uranyl borates that we have prepared, we have not observed BO_4 units between the layers. In **NaUBO-4**, the BO_3 units are linked together to yield a rather open structure. This structure is depicted in Figure 1b, and if one follows the polymerized BO_3 units, both bending and twisting can be seen. This helical feature reduces the interlayer space and provides a less open and presumably more stable structure than would be achieved if the BO_3 units were coplanar. Again, this feature is consistent with the noncentrosymmetric nature of these compounds. Given that **NaUBO-4** can be prepared as a pure phase, we were able to provide external verification of the acentricity by second-order harmonic generation of 532 nm light from 1064 nm laser irradiation.

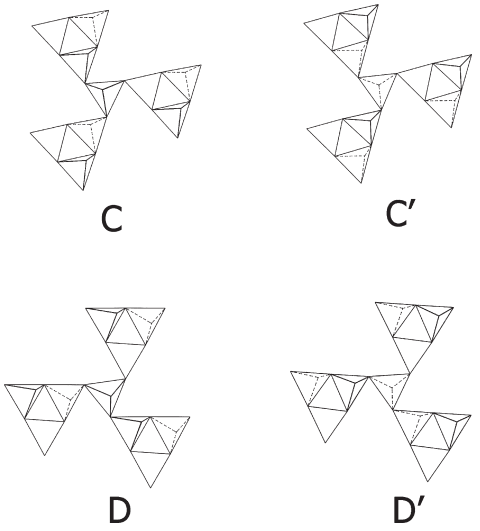

Figure 5. Characteristic fragments of the oxoborate sheets in α-$Tl_2[(UO_2)_2B_{11}O_{18}(OH)_3]$ (**TlUBO-1**), β-$Tl_2[(UO_2)_2B_{11}O_{18}(OH)_3]$ (**TlUBO-2**), $Tl[(UO_2)_2B_{10}O_{16}(OH)_3]$ (**TlUBO-3**), and $Tl_2[(UO_2)_2B_{11}O_{19}(OH)]$ (**TlUBO-4**).

Topological Description of Thallium Uranyl Borates. Within the structures of these compounds we can separate sheets fragments based on 2D polyborate nets and uranyl cations. One of the most interesting structural aspects of these phases is the topology of the polyborates nets within these sheets. There are five main types of topologies (A, B, C, D, and E) and four additional subtypes (A′, B′, C′, D′). As shown in Figure 4, the E topology is unique and realized only in the structure of **TlUBO-1** (vide infra).

The topologies A, B, C, and D (or the related forms A′, B′, C′, D′) are realized in **TlUBO-2**, **TlUBO-3**, and **TlUBO-4**. Fragments of the sheets possess the new topologies showed in Figure 5 (topologies C-C′ and D-D′). In this figure we can see that the C and D topologies are a bit

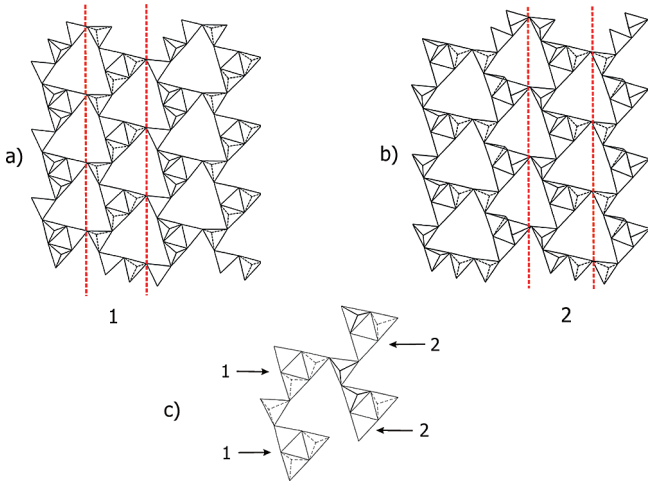

Figure 6. The principal scheme of the formation of the oxoborate sheets in α-$Tl_2[(UO_2)_2B_{11}O_{18}(OH)_3]$ (**TlUBO-1**): (a) sheet fragment in Ba/K-neptunyl borates; (b) sheet fragment in plutonyl borate; (c) characteristic fragment of oxoborate sheet in α-$Tl_2[(UO_2)_2B_{11}O_{18}(OH)_3]$ (**TlUBO-1**).

different from the A and B layers.[10] These sheets are based on the fragments (Figure 2) consisting of one BO_4 tetrahedron (in the center) and three supertriangle groups connected with central tetrahedron by vertices in one plane. Each of the previously mentioned supertriangles consists of one BO_3 flat triangle and two BO_4 tetrahedra. The terminal oxygen atoms in these tetrahedra are oppositely directed (one "up" and one "down"). The symmetrical relationships in the groups of new sheets (for example, C-C′ or D-C′ transformations) are the same as those observed in sodium uranyl borates. All types of layers realized in crystal structures of **TlUBO-2**, **TlUBO-3**, and **TlUBO-4** are polar. Thus, all resulting structures are based on alteration of different polar layers (Figure 1b,c) and are polar too (space group *Cc*). In general the C and D types of sheets are similar with oxo-borate sheets recently observed in $PuO_2[B_8O_{11}(OH)_4]$.[10] The main point of difference between them is the direction of the terminal oxygen atom in the "central" tetrahedron—in Tl-uranyl borates all of these atoms are on one side (all "up" or all "down), but in the plutonyl borate, they alternate, and the resulting sheet is not polar.

As we mentioned above, the topology type E is realized only in the structure of **TlUBO-1**. This topology is more complicated than all others that we have observed before in the chemistry of actinide borates.[10] In Figure 6a,b, we show the fragments of the polyborate sheets we observed in the structures of neptunyl borates and plutonyl borate, respectively.[10] We can separate in both net-types two different fragments. These fragments are shown with red dashed lines in Figures 6a,b (1 for the Np structures and 2 for the Pu structure). If we take these separated fragments and connect them to others with regular alternation in 2D space, then as a result of this operation we obtain complex topology E, realized in **TlUBO-1**. Thus, in this structure two motifs (Np and Pu) are observed simultaneously.

In comparison with Na-based uranyl borates, the Tl-phases are more complicated and diverse. In the structures of the Na-containing uranyl borates, only one type of polyborate sheet with one principal topology variant (four with symmetrical transformations) was found. In the Tl-system, we observed three principal topology variants (nine with symmetrical transformation).

Polymorphism and 2D−{2D-3D}−3D Structural Evolution in Tl-Uranyl Borates. Phases **TlUBO-1** and **TlUBO-2** in the Tl-uranyl borate system are stoichiometrically identical but crystallized in different space groups and possess different structural motifs. The BO_3 and BO_4 units arranged within the oxo-borates sheets in **TlUBO-1** and **TlUBO-2** are quite different as described above. In the structure of **TlUBO-1** only one type of such sheets is realized, but in the structure of **TlUBO-2**, we observe two main topologies and six derivatives of them. The most obvious change is the coupling of sheets in the structure of **TlUBO-2**. As the result of this coupling, the structure of **TlUBO-2** changes from a pure 2D form to an intermediate {2D-3D} state. Diversity in these polymorphic modifications is larger in comparison with the α-$Na[(UO_2)_2B_{10}O_{15}(OH)_5)]$ and β-$Na[(UO_2)_2B_{10}O_{15}(OH)_5]$ polymorphs.

In the final point of the structure descriptions it is necessary to pay attention to structural modification along the line 2D (**TlUBO-1**)−{2D-3D} (**TlUBO-2** and **TlUBO-3**)−3D (**TlUBO-4**). The Tl-uranyl borate family is an example of a system with similar chemical composition and gradually increasing dimensionality. Between the phase **TlUBO-1** (sheet based structure) to **TlUBO-4** (classical 3D material), we have two intermediate states in the form of double layers in **TlUBO-2** and **TlUBO-3** (Figure 4). The coupling of the sheets in **TlUBO-2** goes via single BO_3 triangles (Figure 4b), and in the structure of **TlUBO-3** the sheets are connected by B_3O_5 dimers (Figure 4c). We should mention that doubled layers (consisting of two linked sheets) are rare in actinide chemistry and previously were observed only a few times,[21] but our research on actinide borates substantially expands this group.[10] This is interesting in that in the structure of **TlUBO-4** we can separate fragments of doubled layers identical for both **TlUBO-2** and **TlUBO-3**. The oxo-borate sheets in **TlUBO-4** are connected by BO_3 triangles and B_3O_5 dimers in consecutive order, and as a result form a regular 3D framework (Figure 4).

Details on Coordination and Bonding Metrics in Uranyl Borates. In the previous discussion we have focused on the general crystallographic and topological relationships in the families of sodium and thallium uranyl borates. Here we provide some specific details about bonding and coordination that aid in properly describing these compounds. First, the local coordination environment

(21) (a) Alekseev, E. V.; Krivovichev, S. V.; Depmeier, W.; Siidra, O. I.; Knorr, K.; Suleimanov, E. V.; Chuprunov, E. V. *Angew. Chem., Int. Ed.* **2006**, *43*, 7233–7235. (b) Krivovichev, S. V.; Burns, P. C. *Can. Mineral.* **2003**, *41*, 1455–1462.

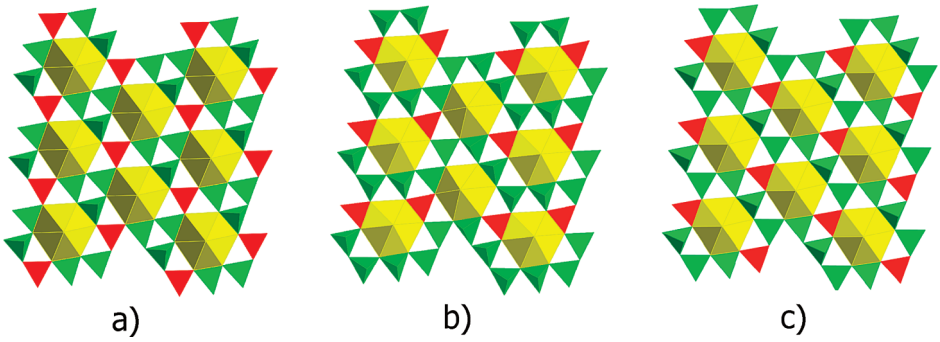

Figure 7. View of the local coordination environment around the uranium atoms in α-**NaUBO-1**, **NaUBO-2**, **NaUBO-3**, and **NaUBO-4** (**a**), **TlUBO-1** (**b**), and **TlUBO-2**, **TlUBO-3**, **TlUBO-4** (**a** and **c**) leading to the formation of sheets. UO_8 hexagonal bipyramids are shown in yellow, BO_3 triangles in red, and BO_4 tetrahedra in green.

around the uranyl units is shown in Figure 7. Here we use color to differentiate between the BO_3 triangles and the BO_4 tetrahedra. The UO_8 hexagonal bipyramid is not a common building unit for uranyl compounds in general.[22] Uranyl compounds are dominated by UO_7 pentagonal bipyramids.[22] However, when small anions that are capable of chelating uranyl are employed, hexagonal bipyramids become much more common. This is known with nitrate and carbonate, for example.[23] Here we show that this general principle holds true with borate. There are nine borate units surrounding each uranyl cation as shown in Figure 7. Six of these units are BO_4 tetrahedra and three of them are BO_3 triangles. Each of the BO_3 units is separated from each other by two BO_4 units.

Given the plethora of bond distances available on uranyl compounds, it would be a misuse of space to provide more details on the bond distances than are already available in the CIF's. However, there are some noteworthy differences between these compounds and most other uranyl compounds. First, the uranyl oxo distances are very short and average 1.79(3) Å in uranyl compounds in general.[24] Some choose to express these bonds as double and some as triple, but we will just leave it with them being short and strong. Normally they are also exactly equal because of imposed symmetry, or close to being equal even when the uranium atom is on a general position. However, such symmetry is not imposed upon the uranyl cations in these compounds. Second, the uranyl units are also slightly bent. Again, symmetry often dictates an O−U−O bond angle of exactly 180°. Here there are slight deviations from linearity by a few degrees, which is not uncommon but is a requirement of the noncentrosymmetric space groups. The bond distances within the equatorial planes surrounding the uranyl units are also irregular, and in **NaUBO-1**, for example, range from 2.389(8) to 2.591(8) Å.

B−O bond distances show substantial variations but are generally notably shorter in the BO_3 triangles than in BO_4 tetrahedra. Protonation of the oxygen atoms leads to noticeable bond lengthening, and B−OH bonds can be identified by both bond length considerations and bond-valence sum calculations.[25]

Finally, there is the question as to why the thallium compounds display far more structural diversity than the sodium phases. There are really two possibilities here. The first is the differences in ionic radii. Tl^+ is considerably larger than Na^+, and there could be as much as a 0.7 Å difference between the radii of these ions. A review of the close contacts between Na^+ and the uranyl borate sheets and frameworks shows that these are typically 0.2 Å shorter than those found with Tl^+. These shorter contacts may allow Na^+ to have a structure-directing effect that is absent in the thallium materials. A second possibility is that the inert lone-pair on Tl^+ has an effect on the structures. We observe no evidence for this.

Conclusions

We have, at last, uncovered a general, synthetic route to actinide borates. The boric acid flux method is a facile and safe way of preparing a large number of actinide borates, two families of which are reported here. The vast majority of these compounds are noncentrosymmetric. In our introduction we focused on two interesting applications of borate compounds, as NLO materials, and as materials for storing nuclear waste. We have demonstrated in this report that both are real possibilities. However, even though kilograms of uranium only represent radiation levels on a μCi scale, scientists and the public in general have been raised in an environment where the mere mention of "uranium" inspires some degree of both fascination and, more importantly, fear. The idea of growing very large crystals of uranium compounds and cutting and polishing them into optics for lasers is unrealistic, and to suggest it as justification for work on actinide borates is disingenuous. There is, however, a caveat to this. These compounds might very well inspire researchers to investigate nonradioactive analogues of uranyl compounds that will lead to real NLO applications. For example, we noted in our studies of actinide iodates that most were centrosymmetric despite the

(22) Burns, P. C. *Can. Mineral.* **2005**, *43*, 1839–1894.
(23) Clark, D. L.; Hobart, D. E.; Neu, M. P. *Chem. Rev.* **1995**, *95*, 25–48.
(24) Burns, P. C.; Ewing, R. C.; Hawthorne, F. C. *Can. Mineral.* **1997**, *35*, 1551–1570.
(25) (a) Brown, I. D.; Altermatt, D. *Acta Crystallogr.* **1985**, *B41*, 244–247. (b) Brese, N. E.; O'Keeffe, M. *Acta Crystallogr.* **1991**, *B47*, 192–197.

presence of an anion with a stereochemically active lone pair of electrons.[26−31] We were able to break the center of symmetry by replacing trans-UO_2^{2+} with cis-MoO_2^{2+} and thereby prepared a family of polar transition metal iodates whose NLO response was on par with some commercial materials.[32]

(26) (a) Weigel, F.; Engelhardt, L. W. H. *J. Less-Common Met.* **1983**, *91*, 339–350. (b) Bean, A. C.; Peper, S. M.; Albrecht-Schmitt, T. E. *Chem. Mater.* **2001**, *13*, 1266–1272. (c) Bean, A. C.; Xu, Y.; Danis, J. A.; Albrecht-Schmitt, T. E.; Runde, W. *Inorg. Chem.* **2002**, *41*, 6775–6779. (d) Sykora, R. E.; McDaniel, S. M.; Wells, D. M.; Albrecht-Schmitt, T. E. *Inorg. Chem.* **2002**, *41*, 5126–5132. (e) Sykora, R. E.; Wells, D. M.; Albrecht-Schmitt, T. E. *Inorg. Chem.* **2002**, *41*, 2304–2306. (f) Bean, A. C.; Albrecht-Schmitt, T. E. *J. Solid State Chem.* **2001**, *161*, 416–423. (g) Bean, A. C.; Ruf, M.; Albrecht-Schmitt, T. E. *Inorg. Chem.* **2001**, *40*, 3959–3963. (h) Sykora, R. E.; Bean, A. C.; Scott, B. L.; Runde, W.; Albrecht-Schmitt, T. E. *J. Solid State Chem.* **2004**, *177*, 725–730. (i) Bean, A. C.; Campana, C. F.; Kwon, O.; Albrecht-Schmitt, T. E. *J. Am. Chem. Soc.* **2001**, *123*, 8806–8810. (j) Shvareva, T. Y.; Almond, P. M.; Albrecht-Schmitt, T. E. *J. Solid State Chem.* **2005**, *178*, 499–504.

(27) (a) Bean, A. C.; Scott, B. L.; Albrecht-Schmitt, T. E.; Runde, W. *J. Solid State Chem.* **2004**, *176*, 1346–1351. (b) Sykora, R. E.; Bean, A. C.; Scott, B. L.; Runde, W.; Albrecht- Schmitt, T. E. *J. Solid State Chem.* **2004**, *177*, 725–730. (c) Bean, A. C.; Scott, B. L.; Albrecht-Schmitt, T. E.; Runde, W. *Inorg. Chem.* **2003**, *42*, 5632–5636. (d) Albrecht-Schmitt, T. E.; Almond, P. M.; Sykora, R. E. *Inorg. Chem.* **2003**, *42*, 3788–3795.

(28) (a) Runde, W.; Bean, A. C.; Albrecht-Schmitt, T. E.; Scott, B. L. *Chem. Commun.* **2003**, *4*, 478–479. (b) Bean, A. C.; Abney, K.; Scott, B. L.; Runde, W. *Inorg. Chem.* **2005**, *44*, 5209–5211.

(29) (a) Runde, W.; Bean, A. C.; Scott, B. L. *Chem. Commun.* **2003**, *15*, 1848–1849. (b) Sykora, R. E.; Assefa, Z.; Haire, R. G.; Albrecht-Schmitt, T. E. *Inorg. Chem.* **2005**, *44*, 5667–5676. (c) Runde, W.; Bean, A. C.; Brodnax, L. F.; Scott, B. L. *Inorg. Chem.* **2006**, *45*, 2479–2482.

(30) Sykora, R. E.; Assefa, Z.; Haire, R. G.; Albrecht-Schmitt, T. E. *J. Solid State Chem.* **2004**, *177*, 4413–4419.

(31) Sykora, R. E.; Assefa, Z.; Albrecht-Schmitt, T. E.; Haire, R. G. *Inorg. Chem.* **2006**, *45*, 475–477.

(32) Sykora, R. E.; Ok, K. M.; Halasyamani, P. S.; Albrecht-Schmitt, T. E. *J. Am. Chem. Soc.* **2002**, *124*, 1951–1957. (b) Shehee, T. C.; Sykora, R. E.; Ok, K. M.; Halasyamani, P. S.; Albrecht-Schmitt, T. E. *Inorg. Chem.* **2003**, *42*, 457–462. (c) Sykora, R. E.; Ok, K. M.; Halasyamani, P. S.; Wells, D. M.; Albrecht-Schmitt, T. E. *Chem. Mater.* **2002**, *14*, 2741–2749.

The more important aspect of this work is perhaps the ability to glimpse into the large glass logs being prepared at Savannah River National Laboratory or the Hanford site for storing nuclear waste. A portion of these glasses has crystallized, but we do not know what these crystals are. This study provides models of how uranyl cations interact with polyborates in the presence of one the most common alkali metal cations found in nuclear waste (Na^+), and these materials are certainly relevant to the vitrification of nuclear waste. We also demonstrated that the pseudoalkali metal Tl^+ is capable of yielding uranyl borate topologies not found with Na^+. Finally, we have shown that this family of compounds is intrinsically interesting owing to the fascinating structures that these compounds adopt that differ in a number of ways from more mundane uranyl compounds. This is reason enough for engaging in this investigation.

Acknowledgment. We are grateful for support provided by the Chemical Sciences, Geosciences, and Biosciences Division, Office of Basic Energy Sciences, Office of Science, Heavy Elements Program, U.S. Department of Energy, under Grants DE-FG02-01ER15187 and DE-FG02-01ER16026, by Deutsche Forschungsgemeinschaft for support within the DE 412/30-2 research project, and under Contract DE-AC02-06CH11357 at Argonne National Laboratory. This material is based upon work supported as part of the Materials Science of Actinides, an Energy Frontier Research Center funded by the U.S. Department of Energy, Office of Science, Office of Basic Energy Sciences under Award Number DE-SC0001089. We thank Professors Gregory S. Girolami and Peter C. Burns for helpful discussions.

Supporting Information Available: X-ray crystallographic files for all compounds (CIF) and powder X-ray diffraction patterns, thermogram, and NLO measurement (PDF). This material is available free of charge via the Internet at http://pubs.acs.org.